Influence of Conformational Dynamics on the Exciton States of DNA Oligomers

Benjamin Bouvier,[†] Jean-Pierre Dognon,[†] Richard Lavery,[‡] Dimitra Markovitsi,*[,†] Philippe Millié,[†] Delphine Onidas,[†] and Krystyna Zakrzewska[‡]

Laboratoire Francis Perrin CEA/DSM/DRECAM/SPAM−CNRS URA 2453, CEA Saclay, 91191 Gif-sur-Yvette, France, and Laboratoire de Biochimie Théorique, CNRS UPR 9080, Institut de Biologie Physico-Chimique, 13, rue Pierre et Marie Curie, 75005 Paris, France

Received: July 24, 2003; In Final Form: September 18, 2003

The present communication examines how the dynamics of the double helix affects the Frenkel excitons that correspond to the low-energy absorption band of DNA. Two types of oligomers, $(dA)_n.(dT)_n$ and $(dAdT)_{n/2}.(dAdT)_{n/2}$, are studied theoretically, in the framework of the exciton theory in combination with quantum chemical calculations. The properties of the exciton states (energy, oscillator strength, degree of delocalization, "anisotropy", etc.) found for canonical B-DNA geometries are compared to those obtained for conformations extracted from molecular dynamics simulations. It is shown that, although structural fluctuations reduce both the mixing between different monomer transitions and the spatial extent of the eigenstates, excitations still remain delocalized over several bases. The presence of alternating base sequences makes the eigenstates of the double-stranded oligomers more sensitive to disorder. All these effects result from a variation of the coupling terms, with the diagonal energy being only slightly altered by the structural fluctuations. The experimental absorption spectra presented here corroborate the theoretical results according to which the absorption of $(dA)_n.(dT)_n$ is centered at higher energies than that of $(dAdT)_{n/2}.(dAdT)_{n/2}$. Finally, it is shown that, in contrast to what is commonly admitted, the formation of collective excited states in double-stranded oligomers is not expected to induce large spectral shifts, with respect to a homogeneous mixture of monomers.

1. Introduction

It is well-known that reactions occurring after the absorption of UV radiation by the DNA bases may induce lethal or carcinogenic mutations. Although the major products of these reactions have been identified,[1] the physicochemical processes that precede DNA damage remain unclear. The very first step in such a series of events is the formation of Franck−Condon excited states. Their nature should determine, in large part, the fate of the excitation energy and, in particular, the possibility for it to be transferred among the bases, thus increasing the efficiency of the photoreactions. In this respect, DNA can be viewed as an organized molecular system that is composed of closely lying chromophores. Therefore, the question arises in regard to whether its electronic excited states are localized on single bases or, more or less, strongly delocalized.

The first communication on DNA excitons appeared in 1960 by Tinoco, who described the excited states of the double helix theoretically by introducing dipolar coupling between the electronic transitions of the bases.[2] On the other hand, experimentalists observed that the spectra of "double-stranded DNA closely resembles the sum of the absorption spectra of the constituent purine and pyrimidine bases" and concluded that "the electronic interaction between the bases is weak enough so that it is proper to speak of the absorption of an ultraviolet photon by a single base".[3] This statement, which guided subsequent studies that involved energy transport,[4−7] implicitly postulates that the formation of exciton states in double helices should induce drastic changes in the profile of the absorption spectra.

The footprint of exciton states in experimental absorption spectra is not always clear, because antagonistic factors may blur the underlying effect. For example, delocalization of the excitation in columnar stacks of chromophores induces a blue shift[8,9] but other geometrical arrangements generate different changes;[10] charge-transfer or charge-resonance interactions induce a red shift in the spectra,[11,12] as does, generally, monomer "solvation" in an organized molecular system. Hence, other observables, such as those obtained by time-resolved spectroscopic measurements, are precious for comparing the behavior of double helices to that of the constituent monomers. Nevertheless, because the excited lifetimes of nucleic acids are extremely short, such measurements were not performed until very recently.[13−17] The first time-resolved investigation of DNA oligomers that was conducted with femtosecond resolution revealed that the molecular organization of nucleotides to form single strands—and, furthermore, to form double helices—slows the fluorescence decays.[18] This observation suggests that important changes may occur in the excited states of the DNA oligomers, as compared to the corresponding monomers, and raises questions concerning the collective excited states in DNA.

In this context, we have recently undertaken a systematic theoretical study of the Frenkel excitons of double-stranded oligomers in close relation with experiments. As a first investigation, we focused on two aspects: (i) the monomer electronic transitions, which must be considered in the construction of the Hamiltonian matrix, and (ii) the dipolar coupling.[19] We determined the energies and transition moments of the lowest dipolar transitions of the individual chromophores that form the double helices by decomposing the absorption

* Author to whom correspondence should be addressed. E-mail: dimitra.markovitsi@cea.fr.
[†] Laboratoire Francis Perrin.
[‡] Laboratoire de Biochimie Théorique.

10.1021/jp036164u CCC: $25.00
Published on Web 11/11/2003

spectra of nucleosides in aqueous solution on the basis of fluorescence anisotropy and circular dichroism measurements. In parallel, we calculated these properties with the CS−INDO−CIPSI method and found a satisfactory agreement with the experimental values. Subsequently, we determined the dipolar coupling using the atomic transition charge distribution model. Finally, we calculated the properties of the exciton states of two particular oligonucleotides, $(dA)_{20}.(dT)_{20}$ and $(dAdT)_{10}.(dAdT)_{10}$, considering three closely lying molecular electronic transitions: two for adenosine and one for thymidine.

The most important conclusion of our first approach was that dipolar coupling may lead to a spatial delocalization of the excitation within double helices that have an idealized B-DNA geometry. But, as noted in that study, the plasticity of the double helix could induce a localization of the electronic excitation. As a matter of fact, a given DNA oligomer can adopt a range of conformations, as a function of time, which may lead to variations of the monomer excitation energy within the organized system (diagonal disorder), as well as the variation of the electronic coupling (off-diagonal disorder). The propensity of structural fluctuations of the double helix to localize the excitation depends on the relative amplitude of the induced diagonal and off-diagonal disorder, compared to the strength of the coupling.

Here, we follow the methodology developed in ref 19, combining exciton theory and quantum chemical methods, to which we add ground state molecular dynamics calculations. In this way, we are able to model structural fluctuations by considering solvent, counterion and temperature effects. We again examine the two types of double-stranded oligomers, $(dA)_n.(dT)_n$ and $(dAdT)_{n/2}.(dAdT)_{n/2}$, which are composed of the same type of base pairs but have, respectively, homopolymeric and alternating base sequences. In Section 2, we describe the procedure that has been followed in the calculations. In Section 3, we present and discuss our results. First, we quantify the amplitude of the diagonal and off-diagonal disorder that is induced by the dynamics of the double helix in the ground state, and we correlate it with the variation of some structural parameters (Section 3.1). We then compare the properties of the Franck−Condon eigenstates (energy, oscillator strength, degree of delocalization, contribution of monomer electronic transitions) obtained with and without structural fluctuations, and we address the problem of the "anisotropy", which should result from intraband scattering (Section 3.2). In Section 3.3, we present the absorption characteristics of $(dA)_n.(dT)_n$ and $(dAdT)_{n/2}.(dAdT)_{n/2}$ oligomers by examining, in parallel, calculated properties and the profile of experimental steady-state absorption spectra. Our conclusions and comments are presented in Section 4.

2. Calculation Procedure

A molecular dynamics simulation of the ground state double helices, including solvent effects and counterions, was used to sample conformational space. The excited states of instantaneous conformations chosen from this simulation were then characterized using an effective Hamiltonian formalism.

2.1. Ground State Molecular Dynamics Simulation. Model building and simulations were performed using the AMBER 6 program[20] and the Parm98 parameter set.[21] Both oligomers were constructed using a standard B-DNA conformation and were subsequently neutralized with 22 Na^+ ions (placed using electrostatic potentials) and solvated with more than 6000 TIP3P water molecules in a truncated octahedral box. Molecular dynamics simulations were performed at constant temperature (300 K) and pressure (1 bar), using the Berendsen algorithm.[22] An integration time step of 2 fs was used, and all bond lengths that involved H atoms were constrained using the SHAKE algorithm.[23] Long-range electrostatic interactions were treated using the particle mesh Ewald (PME) approach[24] with a direct space cutoff of 9 Å. The nonbonded pair list was updated heuristically, and the center-of-mass motion was removed every 10 ps during the simulation. Initially, the water molecules and ions were relaxed by energy minimization and allowed to equilibrate at 300 K around the fixed DNA for 100 ps at constant volume; the entire system was then heated from 100 K to 300 K in 10 ps and equilibrated during 40 ps with harmonic restraints of 5.0 kcal $(mol\ Å^2)^{-1}$ on the solute atoms at constant volume. Subsequently, the simulation was continued at constant pressure; the restraints were gradually removed over a period of 250 ps and an unrestrained simulation followed for >4 ns. The coordinates were saved every 1 ps. The last nanosecond was used for the further study. One hundred snapshots, spaced by 10 ps, were generated. To minimize the bond-length and valence angle distortions, the snapshots were minimized in the AMBER program for 1000 cycles before being used for Poisson−Boltzmann calculations of the electrostatic energy.

2.2. Calculation of Exciton States. *2.2.1. Effective Hamiltonian Formalism.* The excited states of double-stranded DNA fragments are calculated in the framework of the exciton theory,[25−27] in which the exact Hamiltonian of an *n*-molecular supersystem may be written as

$$H = H_0 + V \tag{1}$$

H_0, which is the unperturbed Hamiltonian of the supersystem, is evaluated as the sum of the individual Hamiltonians of the isolated molecules. As a consequence, the zeroth-order eigenfunctions of the system consist of products of the eigenfunctions of these molecules:

$$H_0 = \sum_{\text{molecules } k}^{n} H_k \tag{2a}$$

and

$$|\Phi_m^i\rangle = \Psi_m^i \prod_{\text{molecules } k \neq m}^{n} \Psi_k^0 \tag{2b}$$

where Ψ_m^i denotes the *i*th excited state of chromophore *m*. The excited states of the supersystem are thus decomposed on diabatic states for which the excitation is localized on a given monomer, the other molecules being in their respective ground states.

V is the perturbation operator, which was formalized by Longuet-Higgins,[28] using a local charge density operator $\rho^{(k)}(\vec{r}^{(k)})$ that was associated with each individual chromophore *k*:

$$V = \int\int \frac{\rho^{(k)}(\vec{r}^{(k)})\rho^{(l)}(\vec{r}^{(l)})}{|\vec{r}^{(k)} - \vec{r}^{(l)}|}\, \mathrm{d}\vec{r}^{(k)}\, \mathrm{d}\vec{r}^{(l)} \tag{3}$$

Diagonalization of the exciton matrix *H* in the basis formed by the eigenfunctions of H_0, at the first order of perturbation, yields *N* eigenstates $\Gamma_k = \sum_{\text{molecules } m} \sum_{\text{states } i} C_{k,m}^i |\Psi_1^0 \Psi_2^0 ... \Psi_m^i ... \Psi_n^0|$. The squares of the linear combination coefficients $C_{k,m}^i$ represent the contribution of the diabatic basis wave function $|\Phi_m^i\rangle$ to the adiabatic system eigenstate $|\Gamma_k\rangle$.

2.2.2. Diagonal Exciton Matrix Elements. The diagonal element of *H* that is associated with the diabatic basis wave

function $|\Phi^i_m\rangle$ may be expressed as

$$\langle\Phi^i_m|H|\Phi^i_m\rangle = \langle\Phi^i_m|H_m|\Phi^i_m\rangle + \sum_{n\neq m}\langle\Phi^i_m|H_n|\Phi^i_m\rangle + \langle\Phi^i_m|V|\Phi^i_m\rangle$$
$$= \epsilon^i_m + \sum_{n\neq m}\epsilon^0_n + \sum_{n\neq m}E^{i,0}_{m,n} + \sum_{n\neq m}\sum_{\substack{p<n\\p\neq m}}E^{0,0}_{n,p} \quad (4)$$

where $E^{i,j}_{m,n}$ denotes the interaction energy of monomer m in its ith electronic state with monomer n in its jth electronic state, whereas ϵ^i_m is the electronic energy of chromophore m in its ith electronic state, as defined by

$$H_m\Psi^i_m = \epsilon^i_m\,\Psi^i_m \quad (5)$$

Let E_0 be the electronic energy of the system composed of all chromophores in their electronic ground state:

$$E_0 = \sum_m \epsilon^0_m + \sum_m\sum_{\substack{n<m\\n\neq m}}E^{0,0}_{m,n} \quad (6)$$

The diagonal matrix element $\langle\Phi^i_m|H|\Phi^i_m\rangle$ thus becomes

$$\langle\Phi^i_m|H|\Phi^i_m\rangle = E_0 + \underbrace{(\epsilon^i_m - \epsilon^0_m)}_{\text{I}} + \underbrace{\left(\sum_{n\neq m}E^{i,0}_{m,n} + \sum_{n\neq m}\sum_{\substack{p<n\\p\neq m}}E^{0,0}_{n,p}\right)}_{\text{II}} - \underbrace{\left(\sum_{n\neq m}E^{0,0}_{m,n} + \sum_{n\neq m}\sum_{\substack{p<n\\p\neq m}}E^{0,0}_{n,p}\right)}_{\text{III}} \quad (7)$$

Choosing E_0 as the reference energy (formally, $E_0 = 0$), the diagonal matrix element consists of three terms. Term I represents the excitation energy of monomer m from its ground to its ith electronic state. Term II corresponds to the interaction energy of the system in which monomer m is in its ith state and all others are in their respective ground states. It is computed as the electrostatic energy of the system in water by solving the nonlinear Poisson−Boltzmann equation with AMBER atomic charges. In this calculation, atomic charge distributions associated with the excited states of the monomers (whose determination is explained in the next paragraph) were used. Finally, term III is the energy of the ground state system and is calculated by the Poisson−Boltzmann method.

2.2.3. Off-Diagonal Exciton Matrix Elements. Because the charge density operators involved in the perturbation operator V depend exclusively on the coordinates of the individual subsystems, separation of the variables inside the integrand yields, as an expression of the general matrix element of V, the following expression:

$$\langle\Psi^i_n\,\Psi^j_m|V|\Psi^k_n\,\Psi^l_m\rangle = \frac{\langle\Psi^i_n|\rho^{(n)}\vec{r}|\Psi^k_n\rangle\langle\Psi^j_m|\rho^{(m)}\vec{r}|\Psi^l_m\rangle}{|\vec{r}^{(n)} - \vec{r}^{(m)}|}\,\mathrm{d}\vec{r}^{(n)}\,\mathrm{d}\vec{r}^{(m)} \quad (8)$$

This expression may be viewed as an interaction between appropriate transition charges, obtained from a CS−INDO−CIPSI[29] calculation, as explained in ref 19.

Our model incorporates data from both CS−INDO and CASSCF calculations; therefore, the correspondence of monomer states at the two levels must be determined. Electronic transition energies and oscillator strengths computed at the CASSCF level may be found in Table 1, with CS−INDO and experimental values that have been transcribed from our previous work. Although transition energies show important variations between computational methods and with experiments, the agreement between oscillator strength values is much better and leaves little doubt in regard to the correct attribution of states.

TABLE 1: Excitation Energies (E_{Exc}) and Oscillator Strengths (f) Associated with the First Two Transitions of Adenine and the First Transition of Thymine

	CASSCF		CS−INDO		Experiment[a]	
	E_{exc} (cm^{-1})	f	E_{exc} (cm^{-1})	f	E_{exc} (cm^{-1})	f
adenine $S_0\rightarrow S_1$	41500	0.001	37200	0.057	36700	0.05
adenine $S_0\rightarrow S_2$	48700	0.207	39900	0.216	38800	0.24
thymine $S_0\rightarrow S_1$	42300	0.145	36400	0.220	37500	0.24

[a] Values determined for the nucleosides.[19]

2.3. Degree of Delocalization. The localization behavior of the eigenstates is usually expressed by the inverse participation ratio L_k.[30,31] The number of coherently coupled chromophores in a given eigenstate k is given by the participation ratio $N_k = 1/L_k$. When the eigenstates are built on more than one molecular state, L_k is written as[8]

$$L_k = \sum_{\text{molecules } m}\Big[\sum_{\text{states } i}(C^i_{k,m})^2\Big]^2$$

2.4. General Remarks on the Calculation Procedure. The following includes general comments about the calculation procedure used in this work:

(1) Our intention was to obtain the most-accurate results possible. Therefore, in each step of the calculation procedure, we used different ways to describe the monomer properties. Thus, in the calculation of the diagonal disorder that was induced by the structural fluctuations, we used the properties of the bases (adenine and thymine), because the influence of the backbone was considered explicitly in the molecular dynamics simulations. In contrast, for the coupling terms, we used the properties of the nucleosides, which are the effective chromophores. The transition energies and the oscillator strengths considered are those derived from the decomposition of the experimental absorption spectra recorded in aqueous solutions of adenosine and thymidine (Table 1), as described in our previous work.[19]

(2) Molecular dynamics simulations were performed for oligomers with 12 base pairs; however, the exciton matrix was constructed on only 10 base pairs, neglecting the terminal pairs because of spontaneous base-pair dissociation ("fraying"). Thus, all results associated with the excited states of disordered oligomers refer to $(dA)_{10}.(dT)_{10}$ and $(dAdT)_5.(dAdT)_5$. Furthermore, experimental spectra (see Section 3.3) refer to oligomers with 20 base pairs, because shorter oligomers, such as those used in the molecular dynamics simulations, are not stable at room temperature.

3. Results and Discussion

3.1. Structural Fluctuations and Induced Diagonal and Off-Diagonal Disorder. An analysis of the 100 conformations extracted from the last nanosecond of the molecular dynamics trajectories shows that, at room temperature, both $(dA)_{12}.(dT)_{12}$ and $(dAdT)_6.(dAdT)_6$ undergo significant thermal fluctuations, although they can both be classified as belonging to the B-DNA conformational family. Figure 1 illustrates the overall fluctua-

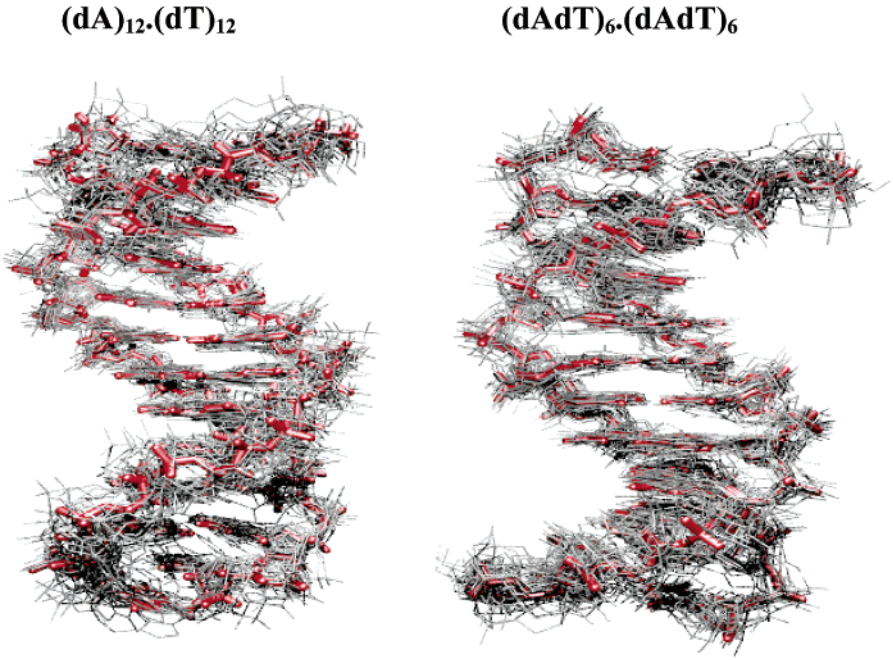

Figure 1. Average structure of the oligomers studied during the last nanosecond of simulation (red) superimposed on 20 representative conformations (gray) chosen from the same part of the trajectory: (a) $(dA)_{12}.(dT)_{12}$ and (b) $(dAdT)_6.(dAdT)_6$.

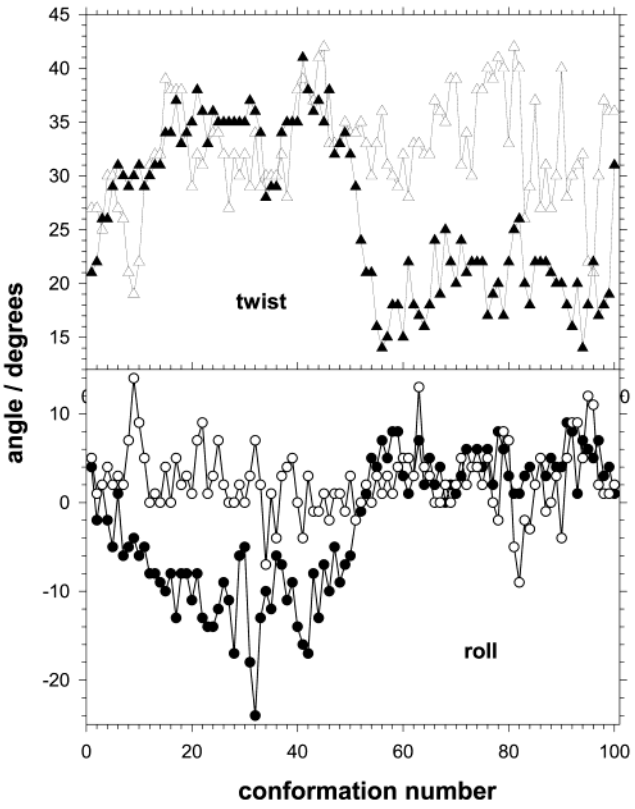

Figure 2. Fluctuations of (a) twist and (b) roll for the A5−A6 step of $(dA)_{12}.(dT)_{12}$ (open symbols) and $(dAdT)_6.(dAdT)_6$ (filled symbols). Twist is the rotation around the helical axis between successive base pairs, and roll is the angle formed between the base-pair planes by rotation around their principal axes (positive roll angles refer to opening up the base pairs on the major groove side of the duplex).

tions by superimposing 20 representative conformations on the average structure obtained from the last nanosecond of simulation.

Figure 2 shows the detailed fluctuations of two helical parameters, twist and roll, for the A5−A6 step of $(dA)_{12}.(dT)_{12}$ and $(dAdT)_6.(dAdT)_6$. Twist is the rotation around the helical axis between successive base pairs, and roll is the angle formed between the base-pair planes by rotation around their principal axes. Positive roll angles refer to opening up the base pairs on the major groove side of the duplex. The twist and the roll obtained for the homopolymeric sequence exhibit fluctuations on a 10-ps time scale of approximately ±10° around mean values of 32.5° and 2.4°, respectively. Similar rapid fluctuations are observed for the alternating sequence. For the latter oligomer, larger and slower fluctuations also occur in twist and roll for the step analyzed. These large fluctuations in local base stacking are often linked to slow conformational changes that occur in the phosphodiester backbones of DNA.

The fluctuations of the diagonal energy induced by the structural fluctuations are very weak; they do not exceed 10 cm^{-1}, that is, 3 orders of magnitude less than the absolute values of the excitation energy (see Table 1). The distribution of the diagonal energy determined for the 10 adenosine and 10 thymidine chromophores in 100 conformations of $(dA)_{10}.(dT)_{10}$ and $(dAdT)_5.(dAdT)_5$ is presented in Figure 3. Note that the broadest distribution is observed for the $S_0 \rightarrow S_1$ transition of thymidine, which is explained by an important change in the atomic charge distributions that are associated with this transition. We also remark that the S_1 states of both adenosine and thymidine are slightly destabilized within the double strands, whereas the S_2 state of adenosine is weakly stabilized.

The fluctuations observed for the off-diagonal terms of the Hamiltonian matrix are much more important than those found for the diagonal terms. An example is given in Figure 4, which shows the dipolar coupling associated with one pair of chromophores for each type of oligomer: the coupling between the $S_0 \rightarrow S_1$ transitions of the 3rd and 4th thymidine chromophores in $(dA)_{10}.(dT)_{10}$ and that between $S_0 \rightarrow S_2$ transitions of the 3rd adenosine located in one strand of $(dAdT)_5.(dAdT)_5$ and the 17th adenosine located in the other strand. In the case of $(dA)_{10}.(dT)_{10}$, the amplitude of the variations in the coupling totals 35%. A more complex pattern is observed for the coupling fluctuations in $(dAdT)_5.(dAdT)_5$: relatively weak variations (amplitudes of $<10\%$) are superimposed on a larger one,

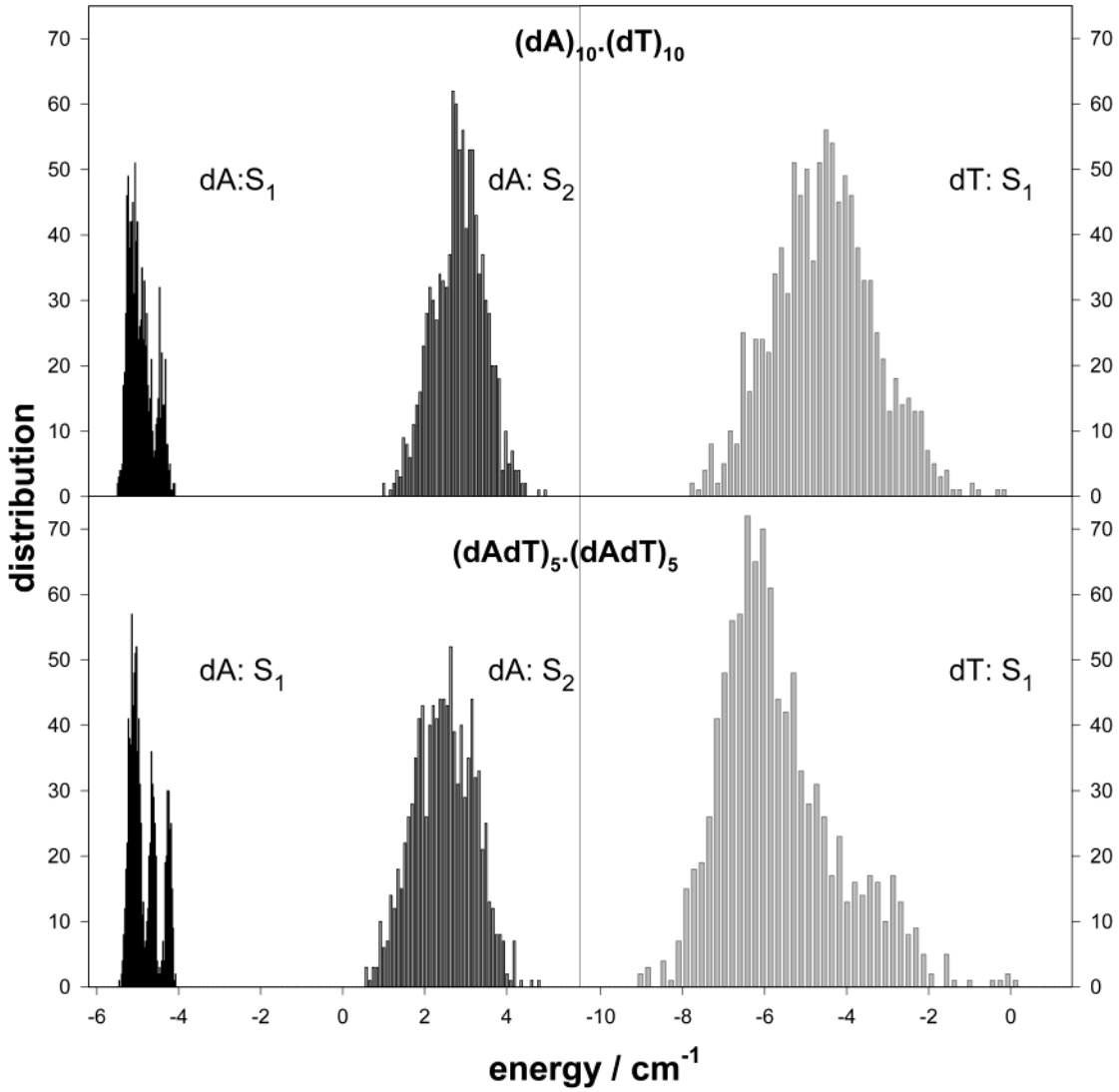

Figure 3. Distribution of the diagonal energy determined for the 10 adenosine and 10 thymidine chromophores in 100 conformations of $(dA)_{10}.(dT)_{10}$ (top) and $(dAdT)_5.(dAdT)_5$ (bottom) extracted from the molecular dynamics simulations.

reaching 45%. This pattern reflects the behavior of twist and roll observed for the alternating oligomer (Figure 2).

3.2. Eigenstate Properties. The eigenstate properties presented here concern exclusively double-stranded oligomers that are composed of 10 base pairs, $(dA)_{10}.(dT)_{10}$, and $(dAdT)_5.(dAdT)_5$. For each type of oligomer, we compare the oscillator strength, the transition energy, the contribution of the monomer transitions, and the participation ratio associated with all 30 eigenstates that have been calculated for perfectly ordered conformations to those found for dynamically disordered conformations. (The structural parameters of ordered oligomers are those which were used in our previous work.[19]) In the latter case, we examine both properties, averaged over an ensemble of 100 conformations, and the behavior of individual conformations.

The distribution of the oscillator strength f over the 30 eigenstates that have been observed for $(dA)_{10}.(dT)_{10}$ is not affected much by structural fluctuations: for both the ordered conformation and the disordered conformations, 90% of the oscillator strength remains concentrated on the same eigenstates, namely $\langle 18\rangle$, $\langle 19\rangle$, $\langle 20\rangle$, $\langle 28\rangle$, $\langle 29\rangle$, and $\langle 30\rangle$. The picture is different for $(dAdT)_5.(dAdT)_5$, for which disorder tends to disperse the oscillator strength over a larger number of eigenstates; in the absence of disorder, 90% of the strength f is borne by only 7 eigenstates, whereas it is spread over 12 of them under the effect of fluctuations. Despite the dispersion of the oscillator strength over several eigenstates, we observed that, for perfectly ordered conformations of both $(dA)_{10}.(dT)_{10}$ and $(dAdT)_5.(dAdT)_5$, the maximum value of f is borne by eigenstate $\langle 29\rangle$. In the case of $(dA)_{10}.(dT)_{10}$, the latter eigenstate continues to have a predominant role, even in the presence of structural fluctuations. In contrast, the maximum oscillator strength observed for disordered conformations of $(dAdT)_5.(dAdT)_5$ is more frequently associated with eigenstate $\langle 22\rangle$.

The variations in the energy of a given eigenstate of $(dA)_{10}.(dT)_{10}$, as a function of the structural changes, do not exceed ± 100 cm^{-1}, and they are generally smaller for the lowest states. The average energy obtained for each of the 30 eigenstates is depicted in Figure 5. For all types of double-stranded decamers, ordered or disordered, homopolymeric or alternating, we note the existence of three ensembles of 10 eigenstates per oligomer, with abrupt changes in energy at the frontier between any two ensembles. This partition is related to the composition of the eigenstates, that is, the contribution to each eigenstate of the three monomer transitions that are considered in the exciton matrix (i.e., $S_0 \rightarrow S_1$ and $S_0 \rightarrow S_2$ of adenine and $S_0 \rightarrow S_1$ of thymine). The monomer contribution, which is expressed as the sum of the squares of the linear

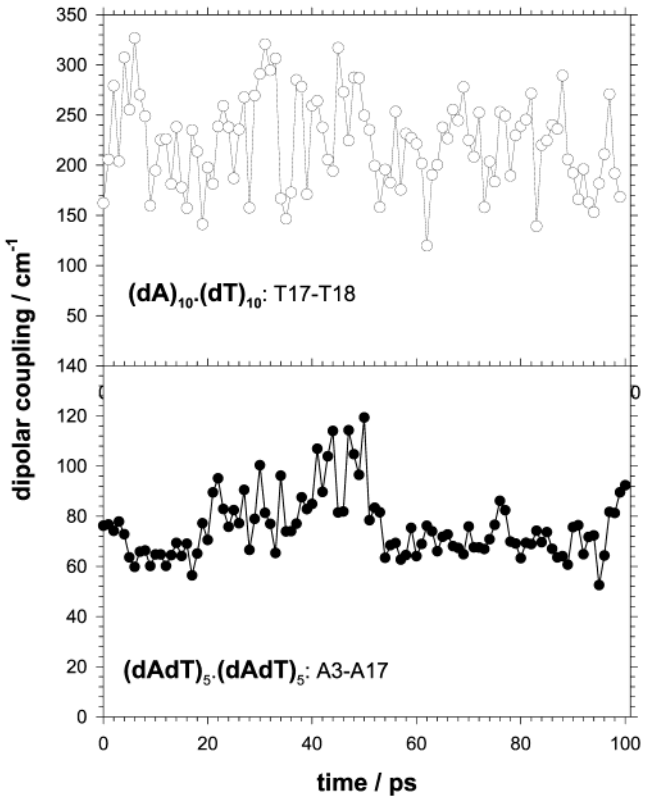

Figure 4. Dipolar coupling determined for 100 conformations extracted from the molecular dynamics simulations. Upper plot shows the coupling between the $S_0 \rightarrow S_1$ transitions of the 17th and 18th thymidine chromophores in $(dA)_{10}.(dT)_{10}$. Lower plot shows the coupling between $S_0 \rightarrow S_2$ transitions of the 3rd adenosine located in one strand of $(dAdT)_5.(dAdT)_5$ and the 17th adenosine located in the other strand.

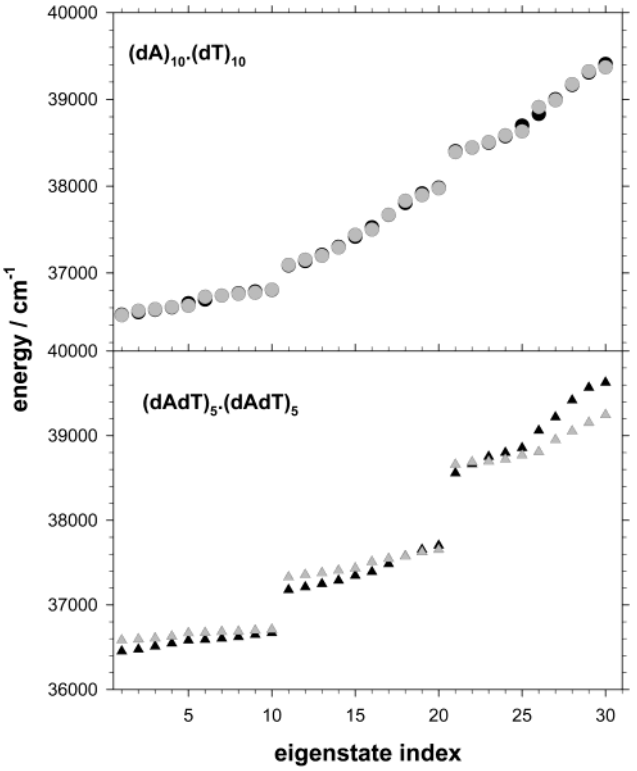

Figure 5. Eigenstate energy determined for (top) $(dA)_{10}.(dT)_{10}$ and (bottom) $(dAdT)_5.(dAdT)_5$. Black symbols represent the average values for 100 conformations extracted from the molecular dynamics simulations, and light gray symbols represent ordered conformations.

combination coefficients, is illustrated in Figure 6. We remark that, exactly as in Figure 5, the 30 eigenstates can be divided into three sets of 10, with each one being associated with a particular monomer transition. The mixing of the monomer transitions is relatively more efficient in the eigenstates of the alternating oligomers; this is true, in particular, for the five upper eigenstates of each set. For both types of oligomer, structural fluctuations tend to reduce the mixing between different monomer transitions; thus, the eigenstates of disordered conformations are built to a larger extent (at least 90% for $(dA)_{10}.(dT)_{10}$ and 75% for $(dAdT)_5.(dAdT)_5$) on a specific monomer electronic state. Thus, the "global" exciton band of each oligomer can be considered to be composed of three "partial" exciton bands. In the case of $(dA)_{10}.(dT)_{10}$, the widths of both the "global" and the three "partial" exciton bands are not altered by structural fluctuations, whereas they decrease for $(dAdT)_5.(dAdT)_5$ (see Figure 5).

In regard to the spatial extent of the eigenstates, a first remark is that none of the eigenstates of the disordered oligomers examined are localized on a single base. The participation ratios are all >2, and, on average, they are in the range of 4−8, depending on the eigenstate index. In Figure 7, we show that, although the average N_k values found for disordered oligomers are relatively high, they are almost all less than the N_k values of the same eigenstates of the corresponding ordered oligomers. We express the reduction of the spatial extent of the excitations induced by structural fluctuations using the quantity $(N_{k,o} - N_{k,d})/N_{k,o}$, where the subscripts d and o designate average disordered and ordered conformations, respectively. This quantity is plotted in Figure 8, where we can see that, for almost all of the eigenstates, the decrease in the participation ratio is larger for the alternating oligomer $(dAdT)_5.(dAdT)_5$. The sensitivity originates from more-important structural fluctuations, leading to greater off-diagonal disorder, as illustrated in Section 3.1.

In the case of ordered oligomers, eigenstates extend along the double strand in a more or less symmetrical and/or periodic manner (cf. Figure 9 in ref 19). As expected, structural fluctuations break down such a regular topography, and different eigenstates may concern different parts of the oligomers. An example is shown in Figure 9, where the bases that participate in eigenstates $\langle 11 \rangle$ and $\langle 1 \rangle$ of the homooligomer and the alternating oligomer are represented in blue and red, respectively.

Finally, we focus on the polarization of the $\langle 0 \rangle \rightarrow \langle k \rangle$ transition that is associated with each eigenstate $\langle k \rangle i$. By analogy with the fluorescence anisotropy used as evidence of excitation transfer in molecular systems, we define the "anisotropy" associated with each eigenstate $\langle k \rangle$, with respect to a reference eigenstate $\langle \lambda \rangle$, as $r_{k,\lambda} = {}^1/_5(3 \cos^2 \theta_{k,\lambda} - 1)$, where $\theta_{k,\lambda}$ is the angle formed between the polarization of the transitions $\langle 0 \rangle \rightarrow \langle k \rangle$ and $\langle 0 \rangle \rightarrow \langle \lambda \rangle$. Figure 10 shows the mean eigenstate "anisotropy" over 100 conformations of $(dA)_{10}.(dT)_{10}$ and $(dAdT)_5.(dAdT)_5$. We note that, for all eigenstates $\langle k \rangle \neq \langle 30 \rangle$, $r_{k,30} < 0.2$. The same result is found if another eigenstate is used as a reference.

Remark: The eigenstate properties presented above have been calculated with the assumption that the monomer electronic transitions are delta functions. In the experimental spectra of the nucleosides in aqueous solution (cf. Figure 2 in ref 19), the absorption bands that correspond to the three electronic transitions considered in the present work greatly overlap. As a result, we expect a much more efficient mixing of the three monomer electronic states within the eigenstates. This effect will tend to increase delocalization, despite a much larger dispersion of the diagonal energy. Regarding the electronic coupling, the terms

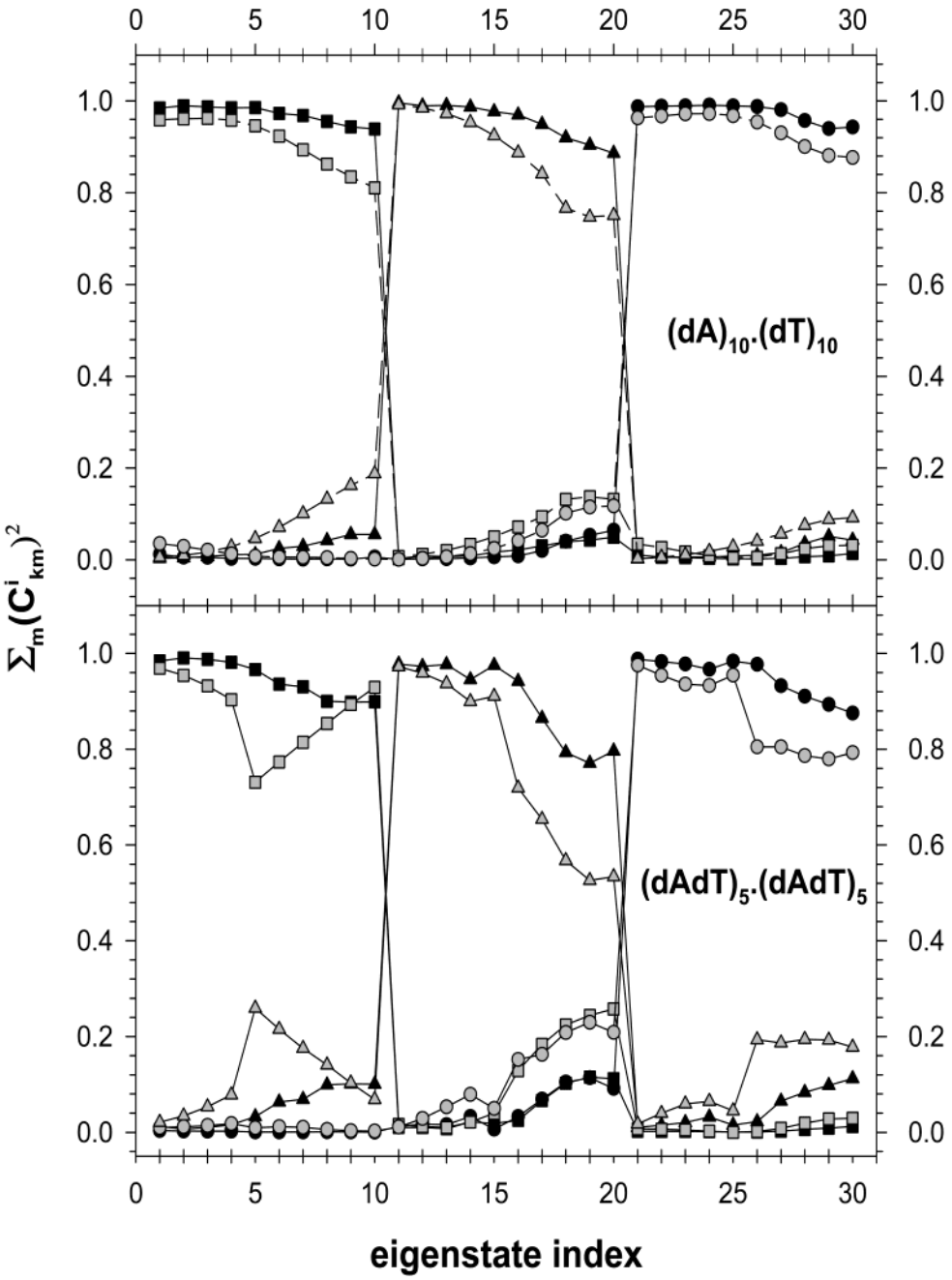

Figure 6. Contribution of the S_1 state of thymidine (triangles) and the S_1 (squares) and S_2 (circles) states of adenosine to the eigenstates of the double-stranded decamers $(dA)_{10}.(dT)_{10}$ and $(dAdT)_5.(dAdT)_5$. Black symbols represent average values extracted from the molecular dynamics simulations, and light gray symbols represent ordered conformations.

that correspond to the edge of the monomer absorption bands would decrease, whereas those which reference the neighborhood of the absorption maximum would increase, thus compensating each other.

3.3. Spectral Properties: Comparison between Theory and Experiment. The absorption "spectra" calculated for $(dA)_{10}.(dT)_{10}$ and $(dAdT)_5.(dAdT)_5$ are represented in Figure 11. They have been simulated by plotting the oscillator strength that corresponds to the 30 eigenstates of one of the 100 disordered conformations. We can distinguish five main "bands" in the $(dAdT)_5.(dAdT)_5$ "spectrum", whereas only four bands appear in that of $(dA)_{10}.(dT)_{10}$.

To quantify the relative position of the calculated "spectra" on the energy axis, we use as a criterion the spectrum barycenter, which is defined as $\nu_b = \sum f_k E_k / \sum f_k$. The ν_b values found for the two types of oligomers, $(dA)_n.(dT)_n$ and $(dAdT)_{n/2}.(dAdT)_{n/2}$, ordered or disordered, are shown in Table 2. They are all located in the energy range of 38 500−39 000 cm^{-1}, that is, a few hundred wavenumbers higher in energy than the value found for the three transitions of the two independent chromophores (38 013 cm^{-1}). We note that, for both oligomers, the structural fluctuations tend to shift the absorption barycenter to lower energies; however, this change is more important with the alternating sequence (356 cm^{-1}) than with the homopolymeric sequence (290 cm^{-1}). An opposite, but smaller, shift is observed when the length of the oligomers is increased from 10 base pairs to 20 base pairs.

In Figure 12, we compare the profiles of the absorption spectra that have been recorded at room temperature for aqueous solutions of $(dA)_{20}.(dT)_{20}$ and $(dAdT)_{10}.(dAdT)_{10}$.[32] It can be

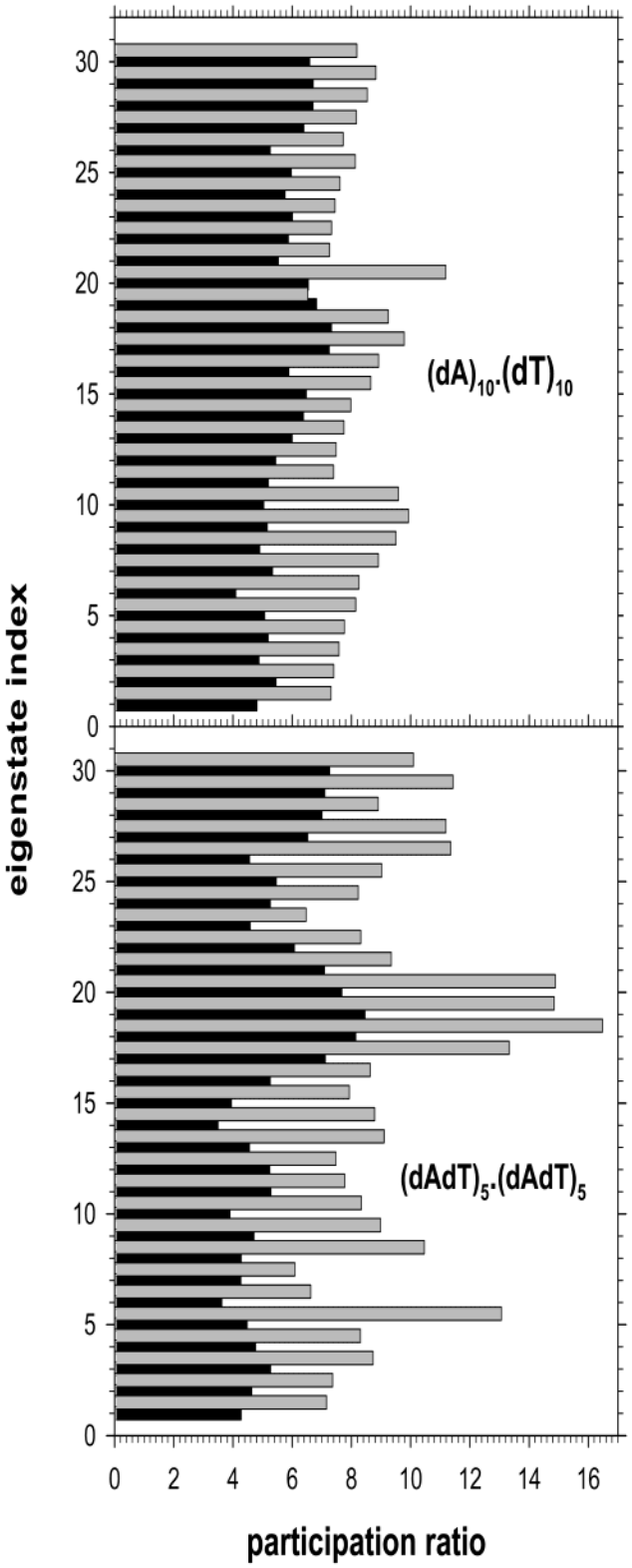

Figure 7. Influence of double-helix dynamics on the participation ratio corresponding to the eigenstates of (top) $(dA)_{10}.(dT)_{10}$ and (bottom) $(dAdT)_5.(dAdT)_5$. Black bars represent the average values for 100 conformations, and light gray bars represent ordered conformations.

clearly seen that the spectrum of the homo-oligomer is hypsochromically shifted with respect to that of the alternating oligomer. The difference of the absorption maxima is 470 cm^{-1}. The absorption maximum of $(dA)_{20}.(dT)_{20}$ is located 412 cm^{-1} toward higher energies, as compared to the absorption maximum of the sum of the monomer spectra (dA + dT). In contrast, in

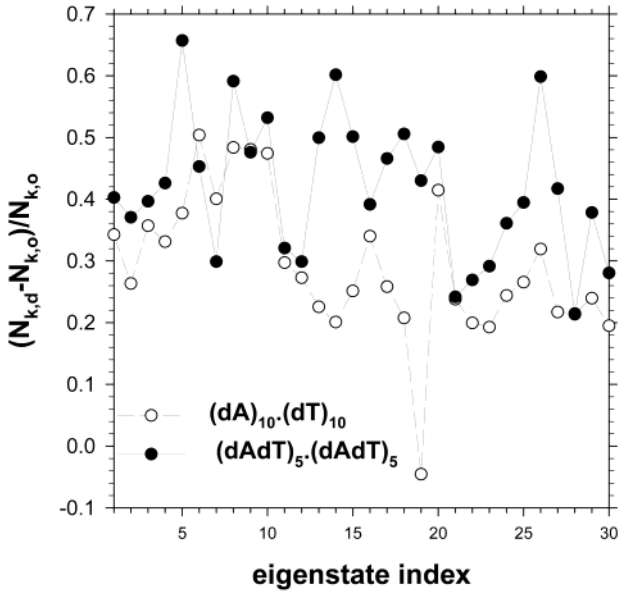

Figure 8. Reduction of the spatial extent of the eigenstates induced by structural fluctuations. N_k is the participation ratio, and the subscripts o and d respectively designate the values obtained for ordered conformations and an average of 100 dynamically disordered conformations.

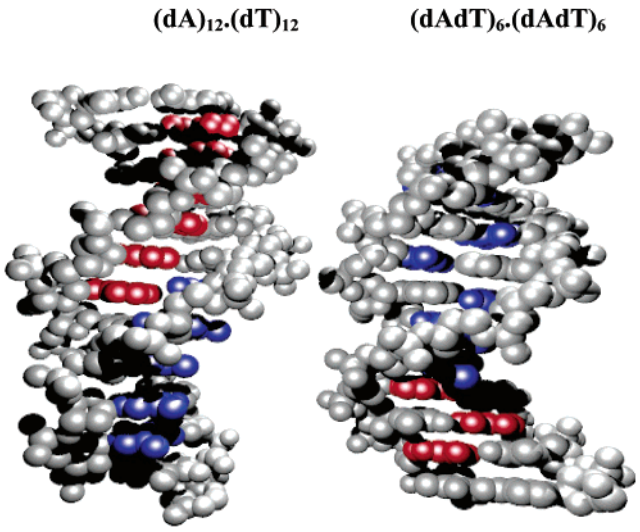

Figure 9. Excited bases corresponding to the eigenstates ⟨11⟩ (in blue) and ⟨1⟩ (in red) of one disordered configuration of the double-stranded homooligomer (left) and the alternating oligomer (right). Oligomers shown correspond to the dodecamers used in the dynamics simulations and, with respect to those used for the calculation of the eigenstate properties, have an additional base pair at each end.

regard to the precision of the measurements, the maximum of the $(dAdT)_{10}.(dAdT)_{10}$ spectrum is the same as that which corresponds to the sum of the monomer spectra.

Prior to any comparison between the calculated and experimental absorption features, we must consider at least two important issues. First, there is a lower limit to the possible agreement between the calculated absorption barycenters and the experimental absorption maxima, which is intrinsic to the manner in which these quantities are determined. This limit can be determined from the difference between the ν_b and ν_{max} values that correspond to the sum of the monomers, both of which are derived from the absorption spectra of aqueous solutions of nucleosides, and is equal to 150 cm^{-1}. Second, the energy of the chromophore transitions used for the determination

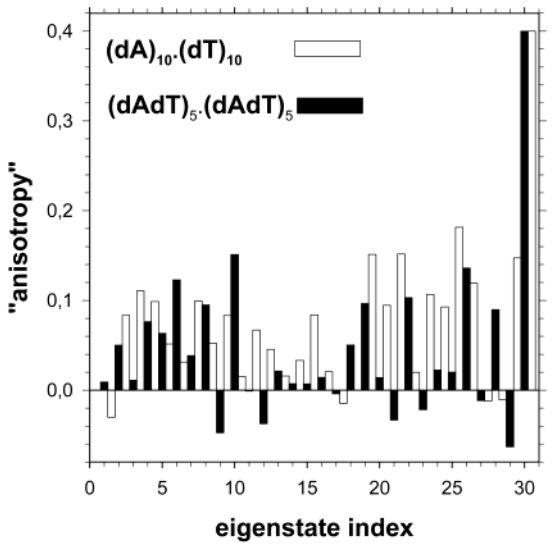

Figure 10. "Anisotropy" associated with each eigenstate $\langle k \rangle$, with respect to the highest eigenstate, $\langle 30 \rangle$. This is defined as $r_{i,30} = {}^1/_5(3 \cos^2 \theta_{i,30} - 1)$, where $\theta_{i,30}$ is the angle formed between the polarization of the transitions $\langle 0 \rangle \rightarrow \langle k \rangle$ and $\langle 0 \rangle \rightarrow \langle 30 \rangle$.

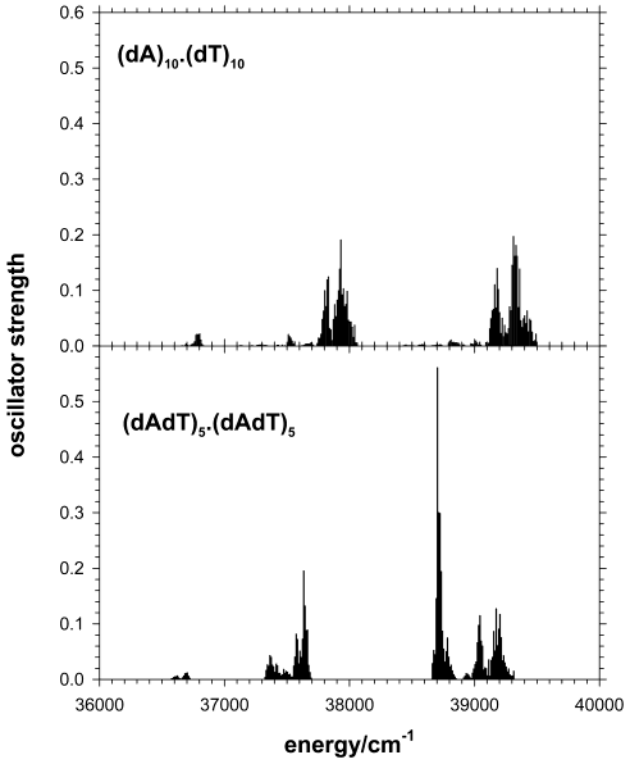

Figure 11. Average absorption "spectra" calculated for 100 conformations of $(dA)_{10}.(dT)_{10}$ and $(dAdT)_5.(dAdT)_5$. The total oscillator strength is normalized per base pair; the width of the individual subdivisions equals 10 cm^{-1}.

of the diagonal terms of the Hamiltonian matrix is that which corresponds to the nucleosides in aqueous solutions and not that which corresponds to the gas phase, because the latter values are not known. However, on the basis of experiments performed for 9-methyladenine, we can estimate that the energy difference between the gas and aqueous phases amounts to a few hundred wavenumbers.[33,34] Third, an increase in the length of the oligomer may induce structural fluctuations of larger amplitude.[35]

With these limitations in mind, our model predicts that the shift of the oligomer spectra, with respect to that of the sum of

TABLE 2: Absorption Characteristics

system	type	barycenter	maxima[a]
dA + dT	experimental[b]	38013	38168
$(dA)_{20}.(dT)_{20}$	experimental		38580
$(dA)_{20}.(dT)_{20}$	ordered	38983	
$(dA)_{10}.(dT)_{10}$	ordered	38891	
$(dA)_{10}.(dT)_{10}$	disordered	38601	
$(dAdT)_{10}.(dAdT)_{10}$	experimental		38110
$(dAdT)_{10}.(dAdT)_{10}$	ordered	38916	
$(dAdT)_5.(dAdT)_5$	ordered	38857	
$(dAdT)_5.(dAdT)_5$	disordered	38501	

[a] Experimental error: ± 30 cm^{-1}. [b] Derived from decomposition of the experimental spectra, as explained in ref 19.

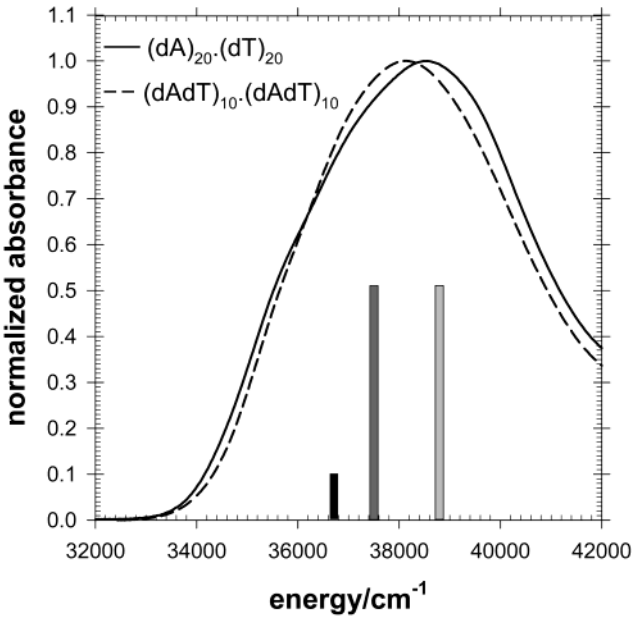

Figure 12. Normalized absorption spectra of (—) $(dA)_{20}.(dT)_{20}$ and (— — —) $(dAdT)_{10}.(dAdT)_{10}$ in aqueous buffered solutions. Vertical bars represent the position and oscillator strength corresponding to the $S_0 \rightarrow S_1$ (black) and $S_0 \rightarrow S_2$ adenosine (light gray) and $S_0 \rightarrow S_1$ thymidine (dark gray) electronic transitions.

the monomers, should not be larger than a few hundred wavenumbers (i.e., ≤ 3 nm in the considered spectral area), which is consistent with experimental observations. Previous theoretical studies predicted a shift of several thousand wavenumbers.[36] Moreover, according to our model, the homopolymeric decamer absorbs at higher energies than the alternating decamers, which is in agreement with the spectra shown in Figure 12. Finally, the relative position of the spectra presented here, as well as the absolute values of the calculated absorption characteristics, are in accord with experiment. In fact, the maxima of experimental spectra of all the oligomers are located in the 38 100−38 600 cm^{-1} range, whereas the barycenters are found in the range of 38 500−39 000 cm^{-1}. This agreement between experimental and theoretical values, which improves when structural fluctuations are considered, is the best observed so far.

4. Conclusions and Comments

The main conclusions of the present work, where the influence of conformational dynamics on the exciton states of DNA oligomers was examined for the first time, can be summarized as follows.

Although structural fluctuations reduce both the mixing between different monomer transitions and the spatial extent

of the eigenstates, excitations still remain delocalized over several bases. Such behavior, which contrasts with the complete charge localization reported quite recently,[37] originates from the nature of the electronic coupling responsible for the formation of Frenkel excitons. Actually, dipolar coupling operates over relatively long distances and is not restricted to nearest neighbors, as is the coupling due to orbital overlap that is associated with charge delocalization. In the presence of structural fluctuations, some interatomic distances that involve different DNA bases increase, but others decrease; consequently, some terms of the dipolar coupling (which is a function of the atomic charge distribution) decrease, whereas others increase, preserving the delocalization of the excitation. The same reasoning could be applied for DNA fragments within nucleosomes, if the electronic structure of the bases is not seriously perturbed by interactions with the core histones.

The sensitivity of the spatial extent of the excitons toward structural fluctuations depends on the base sequence. It would be interesting to examine other sequences to establish general trends regarding this behavior.

The formation of collective excited states in double-stranded oligomers is not expected to induce large spectral shifts, with respect to a homogeneous mixture of monomers. Thus, it is not surprising that collective states are not easily detectable in UV spectra, particularly when these spectra are recorded on a nanometer scale.

Appendix

Calculation of the Excited-State Charges. AMBER charges are only available for ground state bases; therefore, atomic charges for the excited states of the monomers had to be constructed from ab initio calculations. We describe the change in the electronic wave function of the monomers upon excitation as a set of atomic charge differences, computed by subtraction of the CASSCF/RESP charges on the atoms of the ground state molecule from those corresponding to the excited state. These changes are shown schematically in Figure A1 for the three transitions studied. The charges for the excited states of thymine and adenine were obtained by adding the corresponding charge difference to the standard AMBER ground state charges. This should account for the reorganization of the electronic system of the monomers upon excitation, while retaining the generality of the AMBER force field, which is very well-suited to the study of nucleic acids.[38]

In calculations of atomic charge differences, atomic charges for the ground and excited states of the DNA bases adenine and thymine were derived from the electrostatic potential calculated on a grid of points from the corresponding individual state CASSCF electronic wave function, using an extended version of the RESP method.[39]

The points on the grid used for charge fitting belong to an ensemble of fused spheres, centered on atoms and having a radius γR, where R is the atomic van der Waals radius of each individual atom. The grid was generated using an algorithm that was developed by Spackman.[40] A value of $\gamma = 1.4$ was determined to provide the best precision while preventing the so-called "hidden atom" phenomenon, i.e., indeterminations that occur during the fitting procedure.[41] The resulting sets were composed of 4151 points for thymine and 3897 for adenine.

Permanent dipole moments equivalent to the charge distributions were compared with their CASSCF counterparts, to assess the quality of the fit, and may be found in Table A1. Both the norm and the direction of these dipole moments show excellent agreement with the ab initio results.

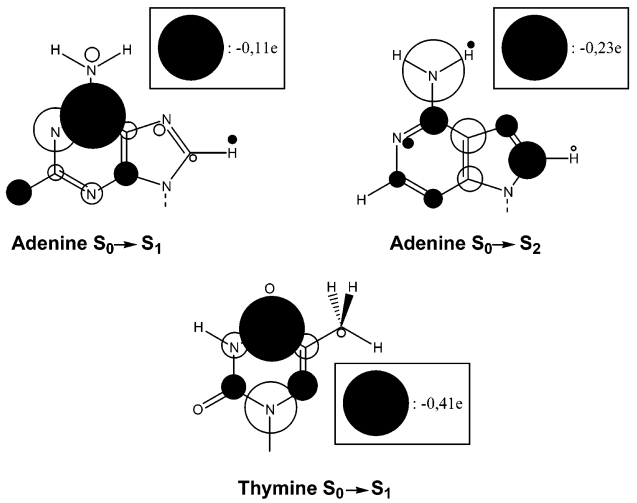

Figure A1. Difference between the excited state and the ground state atomic charges corresponding to the $S_0 \rightarrow S_1$ transition of thymine and the $S_0 \rightarrow S_1$ and $S_0 \rightarrow S_2$ transitions of adenine; negative and positive charges appear as black and white circles, respectively. Circle diameter is proportional to the absolute value of the change in charge.

TABLE A1: Norms ($||\vec{\mu}||$) and Angles (Θ) of the Permanent Dipole Moments of the Electronic States of Adenine and Thymine

	$\|\|\vec{\mu}\|\|$			Θ^a		
	CASSCF	atomic charge	error (%)	CASSCF	atomic charge	error (%)
adenine S_0	2.42 D	2.42 D	<0.1	−89.6°	−88.9°	0.8
adenine S_1	2.10 D	2.09 D	0.3	−85.7°	−84.3°	1.6
adenine S_2	2.52 D	2.53 D	0.7	−26.0°	−25.6°	1.5
thymine S_0	4.06 D	4.09 D	0.8	−124.1°	−126.0°	1.5
thymine S_1	6.96 D	6.94 D	0.4	−169.2°	−166.4°	1.7

[a] According to the DeVoe−Tinoco convention.[46]

Nonlinear solutions of the Poisson−Boltzmann equation were obtained with the DELPHI program (Version 2.1).[42] An ionic strength of 0.145 was used. Calculations involved 145 grid points, and 80% of the box was filled by the molecule, corresponding to 2.7 grid points per angstrom. The internal dielectric constant was taken as 2, and the external dielectric constant was assumed to be 80. The solvent accessible surface of the molecule was defined using a probe radius of 1.4 Å.

Computational Details of Quantum Chemistry Calculations. The geometry of adenine and thymine, as described by their most abundant tautomeric forms, were optimized at the AM1 level. CASSCF calculations on the monomers (C_s point group, cc-pVDZ basis set[43]) used the π subsystem as the active space (12 electrons in 11 molecular orbitals for adenine, 12 electrons in 10 molecular orbitals for thymine). They were conducted using the MOLPRO 2002 package.[44] The grid of points used to fit the electrostatic potential was created using GAMESS(US).[45] All calculations were run on a Compaq model ES45 AlphaServer workstation. The details on the CS−INDO calculations are given in ref 19.

Acknowledgment. Financial support from the ACI "Physicochimie de la Matière Complexe" is gratefully acknowledged. We thank Dr. Michel Mons for helpful discussions.

References and Notes

(1) Cadet, J.; Vigny, P. The Photochemistry of Nucleic Acids. In *Bioorganic Photochemistry*; Morrison, H., Ed.; Wiley: New York, 1990; p 1.

(2) Tinoco, I., Jr. *J. Am. Chem. Soc.* **1960**, *82*, 4785.
(3) Eisinger, J.; Shulman, R. G. *Science* **1968**, *161*, 1311.
(4) Guéron, M.; Eisinger, J.; Shulman, R. G. *J. Chem. Phys.* **1967**, *47*, 4077.
(5) Rayner, D. M.; Szabo, A. G.; Loutfy, R. O.; Yip, R. W. *J. Phys. Chem.* **1980**, *84*, 289.
(6) Georghiou, S.; Zhu, S.; Weidner, R.; Huang, C.-R.; Ge, G. *J. Biomol. Struct.* **1990**, *8*, 657.
(7) Huang, C.-R.; Georghiou, S. *Photochem. Photobiol.* **1992**, *56*, 95.
(8) Marguet, S.; Markovitsi, D.; Millié, P.; Sigal, H.; Kumar, S. *J. Phys. Chem. B* **1998**, *102*, 4697.
(9) Markovitsi, D.; Gallos, L. K.; Lemaistre, J. P.; Argyrakis, P. *Chem. Phys.* **2001**, *269*, 147.
(10) Kasha, M.; Rawls, H. R.; El-Bayoumi, M. A. *Pure Appl. Chem.* **1965**, *11*, 371.
(11) Scholes, G. D.; Ghiggino, K. P. *J. Phys. Chem.* **1994**, *98*, 4580.
(12) Scholes, G. D.; Harcourt, R. D.; Ghiggino, K. P. *J. Chem. Phys.* **1995**, *102*, 9574.
(13) Pecourt, J.-M. L.; Peon, J.; Kohler, B. *J. Am. Chem. Soc.* **2000**, *122*, 9348.
(14) Peon, J.; Zewail, A. H. *Chem. Phys. Lett.* **2001**, *348*, 255.
(15) Onidas, D.; Markovitsi, D.; Marguet, S.; Sharonov, A.; Gustavsson, T. *J. Phys. Chem. B* **2002**, *106*, 11367.
(16) Gustavsson, T.; Sharonov, A.; Markovitsi, D. *Chem. Phys. Lett.* **2002**, *351*, 195.
(17) Gustavsson, T.; Sharonov, A.; Onidas, D.; Markovitsi, D. *Chem. Phys. Lett.* **2002**, *356*, 49.
(18) Markovitsi, D.; Onidas, D.; Sharonov, A.; Gustavsson, T. *ChemPhysChem* **2003**, *3*, 303.
(19) Bouvier, B.; Gustavsson, T.; Markovitsi, D.; Millié, P. *Chem. Phys.* **2002**, *275*, 75.
(20) Case, D. A.; Pearlman, D. A.; Caldwell, J. W.; Cheatham, T. E., III; Ross, W. S.; Simmerling, C. L.; Darden, T. A.; Metz, K. M.; Stanton, R. V.; Cheng, A. L.; Vincent, J. J.; Crowley, M.; Tsui, V.; Radmer, R. J.; Duan, Y.; Pitera, J.; Massova, I.; Seibel, G. L.; Singh, U. C.; Weimer, P. K.; Kollman, P. A. AMBER 6 program; University of California: San Francisco, CA, 1999.
(21) Cheatham, T. E.; Cieplak, P.; Kollman, P. A. *J. Biomol. Struct. Dyn.* **1999**, *16*, 845.
(22) Berendsen, H. J. C.; Postma, J. P. M.; van Gunsteren, W. F.; DiNola, A.; Haak, J. R. *J. Chem. Phys.* **1984**, *81*, 3684.
(23) Ryckaert, J. P.; Ciccotii, G.; Berendsen, H. J. C. *J. Comput. Phys.* **1977**, *23*, 327.
(24) Darden, T.; York, D.; Pedersen, L. *J. Chem. Phys.* **1993**, *98*, 10089.
(25) Frenkel, J. *Phys. Rev.* **1931**, *37*, 1276.
(26) Rashbah, E. I.; Sturge, M. D. *Excitons*; North-Holland: Amsterdam, 1982.
(27) Davydov, A. S. *Theory of Molecular Excitons*; Plenum Press: New York, 1971.
(28) Longuet-Higgins, H. C. *Proc. R. Soc. London, Ser. A* **1956**, *235*, 537.
(29) Momicchioli, F.; Baraldi, I.; Bruni, M. C. *Chem. Phys.* **1983**, *82*, 229.
(30) Dean, P. *Rev. Mod. Phys.* **1972**, *44*, 127.
(31) Schreiber, M.; Toyosawa, Y. *J. Phys. Soc. Jpn.* **1982**, *51*, 1537.
(32) The nucleotides were purchased from Sigma Aldrich. The double-stranded oligomers $(dA)_{20}.(dT)_{20}$ and $(dAdT)_{10}.(dAdT)_{10}$ were obtained from Eurogentec and were purified by polyacrylamide gel electrophoresis (PAGE). All measurements were performed in a phosphate buffer (pH = 6.8; 0.1 M NaH_2PO_4, 0.1 M Na_2HPO_4, 0.25 M NaCl) at room temperature (20 ± 1 °C). Absorption spectra were recorded using a Perkin Lamba 900 spectrophotometer.
(33) Plutzer, C.; Nir, E.; de Vries, M. S.; Kleinermanns, K. *Phys. Chem. Chem. Phys.* **2001**, *3*, 5466.
(34) Nir, E.; Kleinermanns, K.; Grace, L.; Vries, M. S. d. *J. Phys. Chem. A* **2001**, *105*, 5106.
(35) Ha Duong, T.; Zakrzewska, K. *J. Comput. Chem.* **1997**, *18*, 796.
(36) Miyata, T.; Yomosa, S. *J. Phys. Soc. Jpn.* **1969**, *27*, 727.
(37) Lewis, J. P.; Cheatham, T. E., III; Starikov, E. B.; Wang, H.; Sankey, O. F. *J. Phys. Chem. B* **2003**, *107*, 2581.
(38) Giudice, E.; Lavery, R. *Acc. Chem. Res.* **2002**, *35*, 350.
(39) Levy, B.; Enescu, M. *THEOCHEM* **1998**, *432*, 235.
(40) Spackman, M. A. *J. Comput. Chem.* **1996**, *17*, 1.
(41) Bayly, C. L.; Cieplak, P.; Cornell, W. D.; Kollman, P. A. *J. Phys. Chem.* **1993**, *97*, 10269.
(42) Sharp, K. A.; Honig, B. *Annu. Rev. Biophys. Biophys. Chem.* **1990**, *19*, 301.
(43) Dunning, T. H., Jr. *J. Chem. Phys.* **1989**, *90*, 1007.
(44) Werner, H.-J.; Knowles, P. J.; Amos, R. D.; Bernhardsson, A.; Berning, A.; Celani, P.; Cooper, D. L.; Deegan, M. J. O.; Dobbyn, A. J.; Eckert, F.; Hampel, C.; Hetzer, G.; Korona, T.; Lindh, R.; Lloyd, A. W.; McNicholas, S. J.; Manby, F. R.; Meyer, W.; Mura, M. E.; Nicklass, A.; Palmieri, P.; Pitzer, R.; Rauhut, G.; Schütz, M.; Schumann, U.; Stoll, H.; Stone, A. J.; Tarroni, R.; Thorsteinsson, T. MOLPRO 2002.3; University of Birmingham: Edgbaston, Birmingham, U.K., 2002.
(45) Schmidt, M. W.; Baldridge, K. K.; Boatz, J. A.; Elbert, S. T.; Gordon, M. S.; Jensen, J. H.; Koseki, S.; Matsunaga, N.; Nguyen, K. A.; Su, S.; Windus, T. L.; Dupuis, M.; Montgomery, J. A. *J. Comput. Chem.* **1993**, *14*, 1347.
(46) DeVoe, H.; Tinoco, I. *J. Mol. Biol.* **1962**, *4*, 518.